JCTC Journal of Chemical Theory and Computation

pubs.acs.org/JCTC Article

Excitonic Hamiltonian for Singlet Fission: Beyond a Dimer Model

Published as part of Journal of Chemical Theory and Computation special issue "Developments of Theoretical and Computational Chemistry Methods in Asia".

Supriyo Santra, Amartya Bose,* and Debashree Ghosh*

Cite This: https://doi.org/10.1021/acs.jctc.6c00429 Read Online

ACCESS | Metrics & More | Article Recommendations | Supporting Information

ABSTRACT: The importance of singlet fission as a fundamental process with a variety of implications in energy harvesting cannot be overstated. The challenge is to characterize the energy states of these large singlet fission molecular aggregates that participate in the process. Large dimensionality and essential multiconfiguration nature of the electronic states of interest combine to make accurate *ab initio* calculations prohibitively difficult. We present a spin-resolved tight-binding excitonic model for singlet fission that can be parametrized on the basis of *ab initio* calculations on monomers and dimers of molecules and is highly suitable for the study of aggregates. This excitonic model is then used to solve for the energetics of large aggregates. This coarse-grained model is demonstrated specifically on the pentacene crystal, where we evaluated the spectra and density of states. We show the natural emergence of bands of states in some cases and characterize them. Through an analysis of the participation ratio of the eigenstates, we gain crucial insight into the extent of their multireference character. This method is useful in understanding not just the structure of these extended aggregates but also as a cornerstone for incorporation of vibronic features and simulation of the singlet fission dynamics at a quantum-classical or semiclassical level.

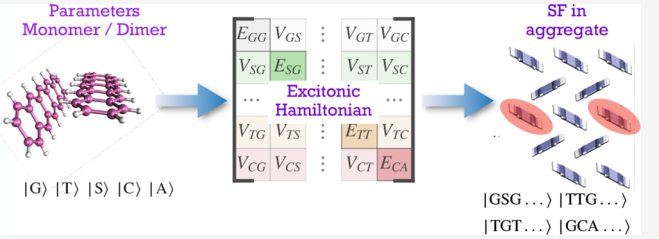

INTRODUCTION

Singlet fission (SF) is a multiexciton phenomenon that produces two triplet excitons on separate molecules/chromophores from a localized exciton created on one molecule or chromophore.[1,2] The process happens via an intermediate state referred to as the triplet pair state or correlated triplet state (^{1}(TT) state). This state conserves the spin of the whole system to a singlet and, therefore, the process becomes spin allowed.[3] The first step of SF phenomena is schematically shown in Figure 1. While the SF phenomenon is typically observed in molecular crystals or aggregates of molecules, the first step requires the molecule to follow the basic energy conservation rule of $E(S_1 - S_0) \geq E(T_1 - S_0)$, when considering the energetics of each molecule (monomer).[1] Due to this energetic restriction, there are only a few molecules that can manifest SF phenomena, and these typically belong to classes of acenes, polyenes, carotenoids, etc.

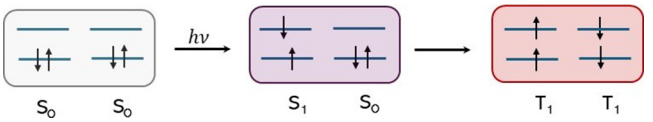

Figure 1. Schematic description of the SF phenomenon. Here, it can be seen that the initial exciton is centered on one monomer (S_1S_0), which subsequently forms two triplet excitons on two monomers through the ^{1}(TT)-pair state.

SF phenomena have been observed to be important in improving the efficiency of solar cells, and especially in circumventing the Shockley–Queisser limit.[4,5] Therefore, it becomes important to understand the electronic structure of the states involved in the phenomena.

Several high-level, accurate calculations have been performed on molecules that are known to undergo SF phenomena. These accounts show that SF phenomena proceed via intermediate states that have significant charge transfer (CT) character in acenes[6−10] and A_g or CT character in carotenoids and polyenes.[11−15] Constrained-DFT calculations revealed substantial CT-state participation in pentacene.[10] This insight prompted subsequent high-level multireference studies on acene crystals and their substituted derivatives.[6,16−19] However, these calculations are on monomer or dimer model systems, while in experiment, most of the observations are typically on much larger aggregates or in crystalline materials. Indeed, it has been observed that the initial excitations of crystalline molecular systems can be quite diffuse and spread out over several monomers.[20,21] TDDFT and

Received: March 6, 2026
Revised: April 7, 2026
Accepted: April 17, 2026

RASSCF level calculations on tetracene derivatives and rubrene show the participation of a minimum of seven monomers.[22] This observation was also in line with those from time-resolved spectroscopy on tetracene.[20] Similar observations were made on pentacene by Head-Gordon and coworkers.[23] By employing QM/MM strategies for pentacene, the important role played by the environment in modulating the SF yield depending on crystal packing was also highlighted.[24] Due to all these reasons, the dimer model and calculations become limited in their scope and interpretation. However, accurate electronic structure on larger oligomers becomes computationally prohibitive.

To circumvent such computational limitations, effective Hamiltonians have been developed and applied successfully to the understanding of several exciton transfer processes.[25−34] Frenkel exciton-like model Hamiltonians have been developed for the SF problem on a diabatic basis.[35−37] While such endeavors circumvent the steep computational cost of *ab initio* calculations on large systems, they are still mired by difficulties with respect to parametrization. Several parametrization approaches have been tried, but it rarely retains physical interpretability and predictive accuracy.[8,9,38] Furthermore, several strategies have been developed to construct effective Hamiltonians for SF process. Fragment-based approaches, such as the active space decomposition method, enable the construction of diabatic Hamiltonians from monomer wave functions and have been successfully applied to molecular dimers to obtain the electronic couplings between diabatic states.[39] More recently, fragment-based nonorthogonal configuration interaction approaches have extended these ideas to larger molecular assemblies and stack geometries.[40] Simplified frontier-orbital Hamiltonians have also been used to gain analytical insight into couplings and to identify favorable intermolecular packing geometries.[41,42] Also, low-rank matrix product state (MPS) representations have been introduced to construct compact Hamiltonians for correlated molecular systems.[43] However, many of these approaches remain limited to small molecular assemblies, and extending them to large aggregates remains a challenge.

Therefore, we develop an excitonic Hamiltonian model suitable for understanding the static and dynamic properties within SF phenomena. We base this excitonic Hamiltonian on a monomer basis to be able to extend the formalism for any size of aggregates. We further incorporate on-site and within-site terms in this Hamiltonian from accurate ab initio calculations that are performed on the monomers and dimers. We benchmark the performance of this method by comparing the spectra of the molecular species in aggregates.

METHOD

Direct electronic structure calculations on SF aggregates become infeasible for large aggregates. We circumvent the problem in two steps − (i) developing a Frenkel exciton-like model Hamiltonian, and (ii) parametrization by accurate electronic structure calculations on monomers and dimers.

Model Hamiltonian

We develop and demonstrate the method for the family of acenes, and pentacene in particular. For SF in aggregates of acenes within a dimer model, the states of importance are the ground state (GS), local excited (LE), CT, and TT states. If we decompose this into monomeric states, we primarily arrive at the ground state ($|G\rangle$), the excited singlet ($|S\rangle$), the triplet state ($|T\rangle$) and the cationic $|C\rangle$ and the anionic $|A\rangle$ states. However, to be able to account for the spin dephasing process, one needs to spin resolve this monomeric basis. This means that we need to include the two spin-resolved cationic ($|C_\uparrow\rangle$ and $|C_\downarrow\rangle$) and anionic ($|A_\uparrow\rangle$ and $|A_\downarrow\rangle$), states and the three triplet states ($|T_{+1}\rangle$, $|T_0\rangle$, and $|T_{-1}\rangle$). We consider all of these states mentioned above as the set of monomeric basis states, the direct products of which are used to construct the entire Hilbert space for the aggregate. Each of the states with multiple spin types would be denoted with two indices, the first for the spin and the second for the monomer number. So, $|T_{sj}\rangle$ would imply the triplet state with spin s at the jth site. The ground and singlet excited states, which do not have different spin variants, would only have a single index corresponding to the monomer number.

The Hamiltonian can be expressed in terms of these states. To motivate the Hamiltonian, let us first understand the structure of the terms:

$$\hat{H} = \hat{H}_{\text{site}} + \hat{H}_{\text{int}} + \hat{H}_{\text{hopping}} + \hat{H}_{S\to C} + \hat{H}_{S\to A} + \hat{H}_{S\to TT} + \hat{H}_{CA\to TT} + \hat{H}_{AC\to TT} \tag{1}$$

where $\hat{H}_{\text{site}}$ are the terms in the Hamiltonian which correspond to the one-body energies of the various states on each of the monomers, $\hat{H}_{\text{int}}$ denotes the two-body interaction energies, i.e., the interaction energy in a CT state refers to the interaction between a cationic and an anionic state residing on different monomers. The hopping of different excitations across the chain without losing their character is described by $\hat{H}_{\text{hopping}}$. In this notation, an example of a two-body singlet spin conformers of charge-transfer states and the triplet-pair states can be written as,

$$\left|{}^1(CA)_{j,k}\right\rangle = \frac{1}{\sqrt{2}}\left(\left|C_{\uparrow j}A_{\downarrow k}\right\rangle - \left|C_{\downarrow j}A_{\uparrow k}\right\rangle\right) \tag{2}$$

$$|{}^1(AC)_{j,k}\rangle = \frac{1}{\sqrt{2}}(|A_{\uparrow j}C_{\downarrow k}\rangle - |A_{\downarrow j}C_{\uparrow k}\rangle) \tag{3}$$

$$|{}^1(TT)_{j,k}\rangle = \frac{1}{\sqrt{3}}(|T_{+1j}T_{-1k}\rangle + |T_{-1j}T_{+1k}\rangle - |T_{0j}T_{0k}\rangle) \tag{4}$$

Using these states, we can provide detailed operator forms for each of the terms in the Hamiltonian.

$$\hat{H}_{\text{site}} = \sum_j \left(\epsilon^{(G)}|G_j\rangle\langle G_j| + \epsilon_j^{(S)}|S_j\rangle\langle S_j| + \epsilon_j^{(T)}\sum_s |T_{sj}\rangle\langle T_{sj}| + \epsilon_j^{(C)}\sum_s |C_{sj}\rangle\langle C_{sj}| + \epsilon_j^{(A)}\sum_s |A_{sj}\rangle\langle A_{sj}|\right) \tag{5}$$

https://doi.org/10.1021/acs.jctc.6c00429
J. Chem. Theory Comput. XXXX, XXX, XXX−XXX

$$\hat{H}_{\text{int}} = \sum_{j<k}\sum_{s,s'} (\epsilon^{(CA)}_{|j-k|}|C_{sj}A_{s',k}\rangle\langle C_{sj}A_{s',k}| + \epsilon^{(AC)}_{|j-k|}|A_{s',j}C_{sk}\rangle\langle A_{s',j}C_{sk}|) + \sum_{j<k}\epsilon^{(TT)}_{|j-k|}\sum_{s,s'}|T_{sj}T_{s',k}\rangle\langle T_{sj}T_{s',k}| + \sum_{j<k}\epsilon^{(GG)}_{|j-k|}|G_jG_k\rangle\langle G_jG_k| + \sum_{j<k}\epsilon^{(SG)}_{|j-k|}|S_jG_k\rangle\langle S_jG_k| + \sum_{j<k}\epsilon^{(GS)}_{|j-k|}|G_jS_k\rangle\langle G_jS_k| \quad (6)$$

$$\hat{H}_{\text{hopping}} = \sum_j h^{(S)}(|S_jG_{j+1}\rangle\langle S_jG_{j+1}| + \text{h. c.}) + \sum_j h^{(T)}\sum_s (|T_{sj}G_{j+1}\rangle\langle G_jT_{s,j+1}| + \text{h. c.}) \quad (7)$$

$$\hat{H}_{S\to C} = \sum_j h^{(SG\to CA)}|S_jG_{j+1}\rangle\langle {}^1(CA)_{j,j+1}| + \text{h. c.} \quad (8)$$

$$\hat{H}_{S\to A} = \sum_j h^{(SG\to AC)}|S_jG_{j+1}\rangle\langle {}^1(AC)_{j,j+1}| + \text{h. c.} \quad (9)$$

$$\hat{H}_{S\to TT} = \sum_j h^{(SG\to TT)}|S_jG_{j+1}\rangle\langle {}^1(TT)_{j,j+1}| + \sum_j h^{(GS\to TT)}|G_jS_{j+1}\rangle\langle {}^1(TT)_{j,j+1}| + \text{h. c.} \quad (10)$$

$$\hat{H}_{CA\to TT} = \sum_j h^{(CA\to TT)}|{}^1(CA)_{j,j+1}\rangle\langle {}^1(TT)_{j,j+1}| + \text{h. c.} \quad (11)$$

$$\hat{H}_{AC\to TT} = \sum_j h^{(AC\to TT)}|{}^1(AC)_{j,j+1}\rangle\langle {}^1(TT)_{j,j+1}| + \text{h. c.} \quad (12)$$

It should be noted that in the interaction terms, long-range interactions are included, and their need, especially for CT states, will be demonstrated later. On the other hand, the hopping terms (eq 7), and the coupling terms to the charge transfer and the triplet pair states (eqs 8−12), include only nearest-neighbor interactions. This nearest neighbor approximation of the couplings is supported by the negligible coupling coefficients obtained for distant dimers. The formalism does not require any such nearest neighbor approximation, and one can easily incorporate distant couplings, albeit with an increased computational cost. Since the ground state (GS) diabat $|G_1G_2\cdots G_N\rangle$ is energetically separated from all excited states in SF phenomena, our approach does not consider coupling with the GS.[6] Furthermore, every state is associated with its character, which determines the singlet excitation component, the triplet excitation, and the charge transfer components in the state. The various populations are calculated as follows.

$$S_{\text{pop}} = \sum_j \langle\psi|S_j\rangle\langle S_j|\psi\rangle \quad (13)$$

$$T_{\text{pop}} = \sum_j\sum_s \langle\psi|T_{js}\rangle\langle T_{js}|\psi\rangle \quad (14)$$

$$CT_{\text{pop}} = \sum_j\sum_s \langle\psi|C_{js}\rangle\langle C_{js}|\psi\rangle \quad (15)$$

Note that the charge transfer population can be calculated as either the cationic population or the anionic population due to the charge neutrality condition that every state satisfies.

Solver

With this Hamiltonian, the size of the Hilbert space is d^N, where d is the number of monomeric states considered ($d = 9$, in this study) and N is the number of monomers. This exponential scaling makes direct computations of large aggregates unfeasible. However, it should be noted that the exponential scaling is only valid when one considers all spin states. Since the SF phenomena occur via singlet, triplet, and quintet states, predominantly, the scaling of such states is polynomial. Furthermore, in most of the benchmark results that we show in this paper, we compare to the absorption spectra, which are purely constrained to the singlet subspace, scales quadratically, thus making exact diagonalization a viable option. We have used exact diagonalization as the solver in all the test cases shown here (we have also implemented DMRG-based solver which can be used when the Hilbert space is truly exponential and we endeavor to target only the low-lying part of the spectra).

Parametrization

The parameters for site energies and the interactions between the monomers are obtained from the accurate *ab initio* calculation on the monomer and dimer geometries taken from the crystal thin film structure as reported in ref 44 (shown in Figure 2a). We focus our discussion on the two prominent directions, the herringbone (Figure 2b) and parallel $\vec{a}$ (Figure 2c) directions. The herringbone and $\vec{a}$ directions are selected based on the crystal packing geometry, as these directions correspond to the dominant nearest-neighbor intermolecular contacts. Interactions along the remaining directions were neglected due to the significantly larger monomer separations and therefore negligible coupling magnitudes (Tables S3 and S4 in Supporting Information).

For parametrizing the Hamiltonian in eq 1, in addition to the one-body terms, *ab initio* calculations on the dimers are also required. We have taken an active space of (4e,4o) comprising HOMOs and LUMOs on each monomer. This suffices to describe all the required states necessary for SF in the case of acenes.[6,8] After localization of the canonical CASSCF orbitals using the Pipek−Mezey scheme,[45] we obtain the diabatic basis. Quantum chemistry software Molpro was used for these calculations.[46] Detailed methods for obtaining the parameters and their magnitudes are given in SI (Section S2). In Figure 3, we show the distance dependence of the energies of various diabats.

First, we discuss the site-based energy terms (eq 5). While the diabatic energies can be obtained from the monomeric calculations, they can also be derived from the dimeric calculations. This is the route we take to ensure greater consistency. To illustrate this, consider the energy of the *GG* diabat as a function of energy, $E_{GG}(r) = \langle GG|\hat{H}|GG\rangle$. This is the black line in Figure 3a. At long distances, the interaction between the two monomers goes to zero. Consequently, $\lim_{r\to\infty}E_{GG}(r) = 2\epsilon^{(G)}$. The same argument is used to obtain the value of $\epsilon^{(T)}$. Now the singlet excitation energy, $\epsilon^{(S)}$ can be obtained as $\lim_{r\to\infty}E_{SG}(r) - \epsilon^{(G)}$. The cationic energy $\epsilon^{(C)}$ is obtained from the monomeric calculations. Finally, to obtain

https://doi.org/10.1021/acs.jctc.6c00429
J. Chem. Theory Comput. XXXX, XXX, XXX−XXX

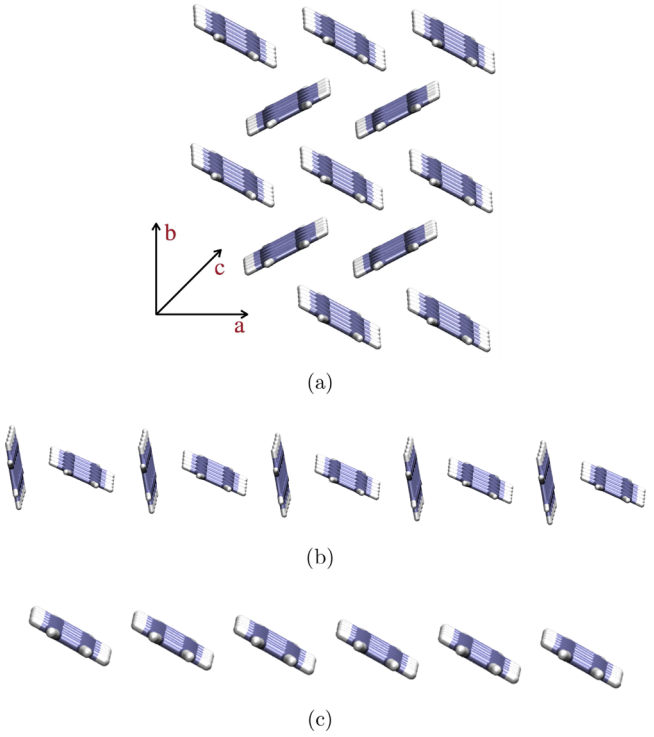

Figure 2. (a) The crystal structure of pentacene. The crystallographic axes are shown (the intermonomer separation along the herringbone and the three crystallographic axes, $\vec{a}$, $\vec{b}$, and $\vec{c}$, are 4.83, 5.98, 7.59, and 15.60 Å respectively.) (b) Aggregate along the herringbone or zigzag direction. (c) Aggregate structure along the *a*-axis.

the energy of the anionic state, we fit the charge-transfer diabatic energy to $E_{\infty}^{(CT)} + E_{corr}^{(CT)}/r$. The anionic value is then obtained as $\epsilon^{(A)} = E_{\infty}^{(CT)} - \epsilon^{(C)}$.

On closer inspection of the diabats, we notice that the correlations in the energies of most of these diabats plateau off within a separation of 2−3 units. However, the distance dependence of the charge transfer diabats, $|CA\rangle$ and $|AC\rangle$, is somewhat sustained. This is to be expected because the asymptotic dependence for these diabats should be the same as Coulomb's interaction, decreasing as $1/r$. For most of the cases, the left−right symmetry is preserved—for example, the energy of the $|SG\rangle$ state is the same as the energy of the $|GS\rangle$ state. The only exception is the large difference in energy of the $|CA\rangle$ and $|AC\rangle$ states at the nearest neighbor herringbone conformation. This owes its origin to multipolar effects generated from asymmetric charge distributions due to the particular conformation in question. From these curves, and using some of the monomeric calculations, it is relatively simple to obtain all the site-based energies, eq 5, and the interaction terms, eq 6.

The interaction terms of eq 6 are now obtained by subtracting the long-distance value of the energy from the corresponding diabatic energy at single lattice separations. For instance, $\epsilon_r^{(GG)} = E_{GG}(r) - 2\epsilon^{(G)}$ or $\epsilon_r^{(TT)} = E_{TT}(r) - 2\epsilon^{(T)}$. The *SG* correlation is obtained as $\epsilon_r^{(SG)} = E_{SG}(r) - \epsilon^{(S)} - \epsilon^{(G)}$. The last *CT* correlation terms are obtained by subtracting $E_{\infty}^{(CT)}$.

For calculation of the coupling and hopping terms (i.e., $h^{(i)}$s in eqs 7−12), we also need the localized orbital description of the dimer states. For the dimer, if $|\psi_i\rangle$ and $|\psi_j\rangle$ represent the two diabatic states, then the coupling between them is given as $\langle\psi_i|\hat{H}|\psi_j\rangle$. The expression of the coupling terms between several diabatic states is taken from the refs 8 and 11. For example, the singlet hopping term $h^{(S)}$ is expressed as $\langle SG|\hat{H}|GS\rangle$, where one singlet exciton has hopped from the monomer on the left to the right. These coupling and hopping terms also decay very rapidly with lattice distance.

To further understand the spectral properties of truly large systems, we have incorporated a periodic boundary condition in our parametrization scheme.

RESULTS

Excited States of Dimers

We have computed the low-lying adiabatic singlet excited states of the dimer, and compared the excitonic Hamiltoninan solution with *ab initio* calculations, 6SA-(4e,4o)-CASSCF/6-31G(d) and RASSCF/6-31G(d). Table 1 presents a comparison of the low-lying excited-state manifold of the pentacene dimer in the herringbone orientation, with the absorption spectrum in SI (Figure S4). There is consistent agreement in the ordering and electronic character of the states between our excitonic approach and the ab initio calculations. The vertical excitation energies (VEEs) are captured with qualitative accuracy. The reason for the slight discrepancies arises from the absence of higher body excitations in the excitonic Hamiltonian. Examples of such excitations are given in the SI (Figure S5). This is also the reason that the excitonic Hamiltonian solution is closer to RASSCF than CASSCF

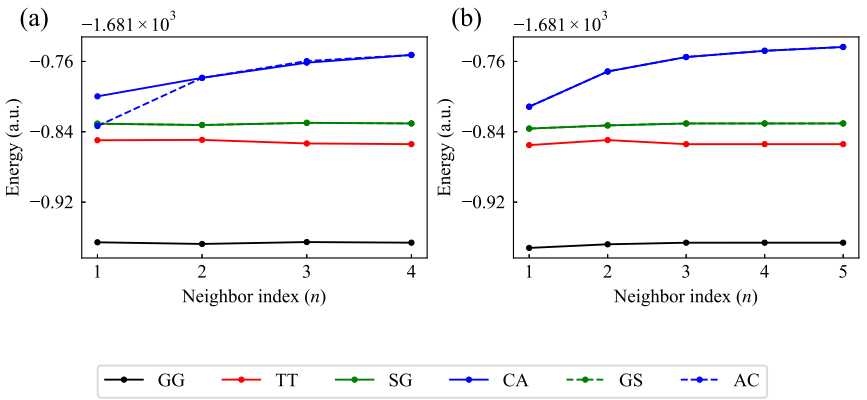

Figure 3. Energies of the dimeric diabatic states as a function of neighbor index (*n*) (a) along herringbone orientation and (b) along $\vec{a}$ orientation. *n* = 1, 2, 3··· corresponds to nearest neighbor, next-nearest neighbor, third nearest neighbor, and so on.

https://doi.org/10.1021/acs.jctc.6c00429
J. Chem. Theory Comput. XXXX, XXX, XXX−XXX

Table 1. Comparison of the Excited States from our Method and (4e,4o)-CASSCF and RASSCF Calculation along Herringbone Orientation[a]

state	nature	SA-6-(4e,4o)-CASSCF	SA-6-(4e,4o)-RASSCF	our method
S_1	TT	3.53 (0.00)	3.40	3.14 (0.00)
S_2	LE + CT	3.81 (0.38)	3.66	3.48 (0.18)
S_3	LE	3.86 (0.16)	3.78	3.64 (0.14)
S_4	LE + CT	4.07 (0.15)	3.92	3.80 (0.28)
S_5	CT	4.90 (0.01)	4.68	4.55 (0.00)

[a]The excitation energies are in eV. Numbers in parenthesis indicate oscillator strengths.

results. However, despite this obvious simplification, the restricted set of diabats captures the essential physics pertinent to the phenomena.

We obtain the nature of the states by analyzing the quantities S_{pop}, T_{pop} and CT_{pop} defined in the previous section. Table 1 shows that the excited states of the pentacene dimer in herringbone orientation exhibit significant mixing between LE and CT character across a large part of the low-lying manifold. Therefore, all the states have moderate optical brightness except for the first excited state, which is predominantly a TT-pair state and, therefore, dark. This LE−CT mixing in the herringbone geometry can be understood as a result of the near-degeneracy of the $|SG\rangle/|GS\rangle$ diabat and the $|CA\rangle$ diabat shown in Figure 3a. The mixed character of the eigenstates results from a combination of coupling between the diabatic states and their energetic proximity.

The nature of the excited states, along the parallel orientation remain quite distinct (Table S3 in Supporting Information). This is expected since the separation of the two monomers being 5.98 Å. The lack of mixing of the CT states with the LE and TT states makes this orientation of the molecules less significant for the SF activity, as was also observed in several previous accounts.[16,24,47,48]

Spectra of Linear Oligomeric Chains

After validating the methodology on dimeric systems, we extend it to investigate the optical spectra of one-dimensional linear aggregates. The model is systematically enlarged by adding one molecular site at a time along each direction independently, and spectral convergence is monitored at every stage. This incremental construction allows us to isolate and quantify the impact of aggregation along each direction on the resulting spectral features.

As a representative case, we analyze the excited state and the spectra of a decamer aggregate extended along the herringbone direction. The resulting low-energy excited state manifold is characterized by strong mixing among LE(S), charge transfer (as, CA/AC), and multiexcitonic triplet (T) configurations. The lowest-lying states are predominantly optically dark and are mainly composed of TT configurations, already exhibiting a finite admixture of CT components. Several states in the 1.8−1.9 eV energy window display pronounced LE−CT hybridization despite carrying only weak oscillator strengths. In contrast, the brightest absorption feature at 1.85 eV arises from coherent superpositions of LE determinants delocalized over multiple sites. At higher energies, a dense manifold of closely spaced states with alternating bright and dark character emerges, accompanied by increasing participation of CT configurations, reflecting progressive electronic delocalization and enhanced interstate mixing within the aggregate. Some of the eigenstates, along with the energies and majorly contributing configurations, are shown in Table 2. The

Table 2. Selected Excited States of the Decamer Aggregate[a]

excitation energies (eV)	f_{norm}	LE	CT	TT	dominant determinants
TT-Dominated States					
1.71	0.004	0.02	0.06	0.91	GGGGGGGGTT (0.91), GGGGGGGGCA (0.06), GGGGGGGTGT (0.02)
1.72	0.003	0.02	0.04	0.92	TTGGGGGGGG (0.92), CAGGGGGGGG (0.04), TGTGGGGGGG (0.02)
1.94	0.000	0.17	0.03	0.76	GGGGGGTTGG (0.37), GGTTGGGGGG (0.22), GGGGGTTGGG (0.14)
1.94	0.000	0.05	0.02	0.87	GGTTGGGGGG (0.30), GGGTTGGGGG (0.20), GGGGTTGGGG (0.14)
Bright LE-Dominated States					
1.85	1.000	0.68	0.22	0.00	GGGGGSGGGG (0.13), GGGGSGGGGG (0.13), GGGGGGSGGG (0.10)
1.92	0.369	0.95	0.00	0.00	GGGGSGGGGG (0.23), GGGGGSGGGG (0.23), GGGSGGGGGG (0.17)
1.96	0.244	0.91	0.07	0.00	SGGGGGGGGG (0.72), GSGGGGGGGG (0.16), CAGGGGGGGG (0.05)
CT-Dominated States					
2.32	0.005	0.01	0.91	0.00	GGACGGGGGG (0.18), GGGGACGGGG (0.18), GGGACGGGGG (0.17)
2.36	0.002	0.00	0.90	0.06	GGGGGACGGG (0.22), GGGACGGGGG (0.18), GGACGGGGGG (0.13)
2.37	0.001	0.00	0.94	0.05	GGGGGGGCAG (0.54), GGGGGGGACG (0.41), GGGGGGGTTG (0.05)
2.54	0.580	0.27	0.71	0.00	GGGGCAGGGG (0.32), GGGCAGGGGG (0.31), GGGGGCAGGG (0.28)

[a]Excitation energies (E) are in eV and oscillator strengths (f_{norm}) are normalized to the brightest transition. LE, CA, and TT denote local excitation, charge-transfer, and triplet−triplet character (squared weights). Only the three dominant determinants are shown for clarity.

presence of multiple closely spaced LE−CT mixed states facilitates the population transfer into correlated TT-pair states. This distributed LE−CT−TT mixing across several excited states highlights the important role of herringbone aggregation in enabling SF in pentacene.

The stick spectrum of the decamer along the herringbone direction is shown in Figure 4a. A uniform energy shift of 1.64

https://doi.org/10.1021/acs.jctc.6c00429
J. Chem. Theory Comput. XXXX, XXX, XXX−XXX

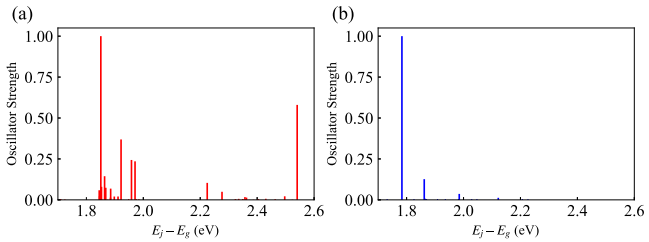

Figure 4. Stick spectrum of the decamer of pentacene along the (a) herringbone and (b) $\vec{a}$ orientation.

eV is applied to align the brightest calculated transition with the corresponding experimental peak. Such a shift is necessary to account for the dynamic correlation that is missing in the parametrization scheme. The dominant absorption feature is centered at approximately 1.85 eV, accompanied by weaker transitions in the 1.9 eV region. This trend is consistent with the state analysis summarized in Table 2. In addition, a higher energy peak appears near 2.5 eV which, although predominantly CT in character, retains a noticeable admixture of LE components.

In contrast, the spectrum along the $\vec{a}$ orientation (Figure 4b) is dominated by a single intense peak at 1.9 eV. Notably, the smaller satellite features observed in the herringbone direction are absent here. This shows reduced mixing of LE and CT configurations and suggests weaker interstate coupling along the $\vec{a}$ direction, implying that this orientation plays a less significant role in facilitating the SF process.

Although the decamer results offer qualitative insight into the excited state character, the associated spectra are not fully converged. We therefore compute spectra for larger oligomers along both the herringbone and $\vec{a}$ directions. As the system size increases, the spectral features sharpen, and at the 100-mer limit, three well-defined peaks emerge, indicating convergence toward the extended aggregate limit (Figure 5a). However, the

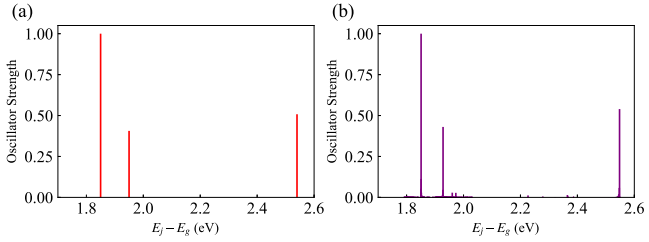

Figure 5. Comparison of the pentacene spectrum of (a) a 1D chain of 100-mer along the herringbone direction and (b) a (8 × 8) 2D lattice.

spectra along the $\vec{a}$ direction has only one bright peak around 1.8 eV, all the other peaks disappear in the bulk limit. This comparison with experiment is shown in Table 3 with the experimental numbers taken form ref 5. Here, it is important to note that, if one performs TDDFT calculations, it is only possible for much smaller aggregate sizes, and only a few low-lying states can be targeted. On performing such a calculation, a bright peak is obtained at 1.98 eV. Furthermore, none of the states obtained could correctly depict the TT pair states. Also, it should be noted that TDDFT is known to underestimate CT states, leading to incorrect state ordering and limited mechanistic insights. The excited states again exhibit mixed LE and CT character, with the lower energy states being

Table 3. Comparison of the Bright Excited States for the 100-mer Aggregate along Herringbone Orientation and along $\vec{a}$ Direction with the Experiment[a]

1D-100 mer ($\vec{a}$)	1D-100 mer (herringbone)	experiment
1.85 (1.00)	1.85 (1.00)	1.85 (1.00)
	1.95 (0.41)	1.97 (0.37)
	2.54 (0.51)	2.13 (0.52)

[a]The energies are in eV and f_{norm} are shown in the bracket.

predominantly LE-like, whereas CT contributions become increasingly dominant at higher energies.

Periodic boundary conditions (PBC) were applied to remove finite-size edge effects and restore translational symmetry within the aggregate. Although the qualitative nature of the spectra remains unchanged, PBC significantly accelerates spectral convergence with respect to system size. A sequential convergence study (Figure S6, in Supporting Information) shows that the excitation spectrum is effectively converged within 30−40 monomers.

Spectra of 2D Oligomeric Systems

Having analyzed the spectral features of the one-dimensional aggregates, we now extend our study to two-dimensional assemblies spanned by $\vec{a}$ and herringbone direction. While the 1D models capture the essential excited-state characteristics along individual directions, inclusion of couplings in both directions, in 2D provides a more realistic description of the aggregate and allows us to assess how additional intermolecular interactions modify the spectra and state mixing.

In Table 4 and Figure 5, the (8 × 8) 2D aggregate spectrum is compared to the converged 100-mer spectra in 1D along the

Table 4. Comparison of the Bright Excited States for the 100-mer Aggregate along Herringbone Orientation and in a (8 × 8) Lattice[a]

1D-100 mer	(8 × 8)-2D
1.85 (1.00)	1.85 (1.00)
1.95 (0.41)	1.92 (0.43)
2.54 (0.51)	2.54 (0.54)

[a]The energies are in eV and f_{norm} are shown in the bracket.

herringbone direction. We observe that the spectral features are remarkably similar, showing that the interactions and spectra are driven by the herringbone direction only.

Nature of States

Figure 6 shows the characterization of the excited states manifold together with their diabatic composition along both crystallographic directions of the aggregate. A clear directional dependence is observed. Along the herringbone direction, mixing between the LE and CT subspaces appears in the low energy region around 1.9−2.4 eV. In addition, CT−TT mixing is evident in the 1.7−1.9 eV region for the herringbone orientation. In contrast, along the parallel ($\vec{a}$) direction, the low-energy states in the same window remain almost purely LE in character. CT-dominated states emerge only above 2.5 eV and are energetically separated from both the LE and TT manifolds. The CT−TT mixing seen in the herringbone case is largely absent in the parallel direction. This behavior reflects weaker intermolecular charge-transfer interactions along $\vec{a}$.

https://doi.org/10.1021/acs.jctc.6c00429
J. Chem. Theory Comput. XXXX, XXX, XXX−XXX

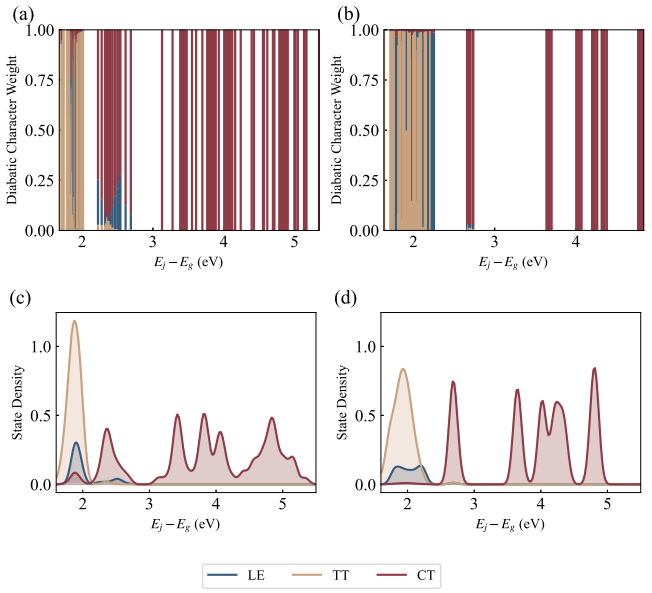

Figure 6. Energy-resolved diabatic character of the excited states for molecular packing along the herringbone (left column) and $\vec{a}$ (right column) directions for a decamer of acenes. Panels (a) and (b) show the discrete eigenstate decomposition, where each vertical bar represents an excited state partitioned into LE, TT, and CT contributions. Panels (c) and (d) display the corresponding character-resolved state densities obtained via weighted histogram broadening with shared normalization.

This anisotropy has direct implications for SF. CT configurations can mediate the coupling between the photoexcited singlet and the correlated TT state. The enhanced LE−CT and CT−TT mixing in the herringbone direction suggests a more effective superexchange pathway and stronger singlet−triplet coupling. These results show the importance of crystal packing for efficient SF phenomena. The same inference can also arrived at from the state densities shown in Figure 6c,d. A similar analysis for 100-mer is given in SI (Figure S7).

To quantify the degree of configurational delocalization, we computed the participation ratio (PR) of each excited state. For an eigenstate expanded in the diabatic basis as

$$|\Psi_j\rangle = \sum_i C_{ij}|\phi_i\rangle \tag{16}$$

the participation ratio is defined as

$$\mathrm{PR}_j = \left(\sum_i |C_{ij}|^4\right)^{-1} \tag{17}$$

This measure reflects the effective number of diabatic configurations contributing to a given state. A value of PR ≈ 1 indicates a localized state dominated by a single configuration, whereas higher values signify larger configurational mixing. The participation ratio is summed across all monomers and is shown for every eigenstate of the aggregate, in Figure 7.

Although the exact PR for the different orientations of the aggregates are different, there are similarities in their trends. The PR of the low-lying states up to 60−70 is high, followed by a region between roughly the 70th and 100th states where the PR shows lower values. For even higher states, we observe significantly low PR. When one considers the nature of the

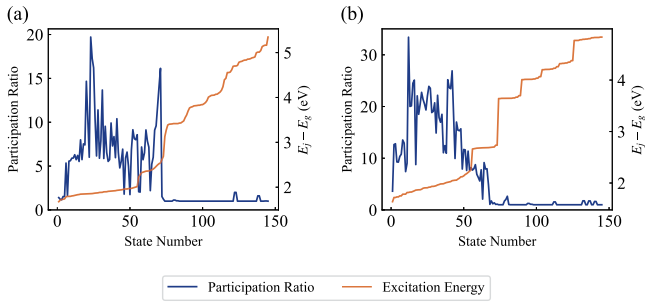

Figure 7. Participation ratio of the 1D decamer of the pentacene aggregate along the (a) herringbone and (b) $\vec{a}$ orientation.

states that these correspond to, we notice that the purely CT states have a low PR. This behavior reflects a transition from strongly mixed low-energy states to predominantly single-configuration charge-transfer states at higher energies. As seen in Figure 7, the reduced PR values in the 70−100 region correspond to states dominated by localized CT character. This is somewhat surprising since they comprise the states given by eqs 2 and 3 in a Bell-like entangled state. However, since these states are entangled only within dimers, the PR is low.

In contrast, LE states in molecular aggregates inherently exhibit multireference character. Describing an exciton requires a coherent superposition of multiple local excitation configurations to capture excitonic delocalization.[28,36,38] This multireference character arises from near degeneracy among local excitation configurations in the excitonic basis.

The energy dependence of the states shows a stepwise increase (Figure 7). These reflect that the states of different natures and multireference character have a propensity to bunch together to form almost band-like structures of states. Though the current work is not about dynamics, this entire analysis sheds light on expectations that one should have when time evolution is taken into account. If we are starting with an excitation into the bright manifold, probably the states that we would be most concerned about are the band near 1.8 eV or the CT-like band up to 2.5 eV. Both these bands are energetically isolated from the extremely high-lying CT states. Moreover, the PR values of those states are also extremely low. This isolation of the bright bands from the high-lying CT states implies that, irrespective of the nonadiabatic couplings between these adiabats, the dynamics would likely be restricted to the manifold below the separation between the CT bands. These ideas would be fully developed in the future once the vibrations are also incorporated through appropriate means.

CONCLUSIONS

In this paper, we have demonstrated that a parametrized form of the aggregate Hamiltonian can be solved to obtain important information about the low-lying electronic states and absorption spectra of singlet fission aggregates. Pentacene has been explored as a particular example system.

For the tight-binding model, one has to choose a diabatic or site-local basis to represent the problem. To ensure both continuity with previous literature and simplicity, we have chosen the ground state $|G\rangle$, the singlet excited state $|S\rangle$, the three triplet states $|T_s\rangle$ and the two cationic $|C_s\rangle$ and anionic $|A_s\rangle$ states as our basis. This is an extension of previous models[6,36,49] used to study singlet fission in the pentacene dimers. Those previous studies have created truncated dimeric

https://doi.org/10.1021/acs.jctc.6c00429
J. Chem. Theory Comput. XXXX, XXX, XXX−XXX

diabatic basis of interest from the five types of states. In our work, we augment the traditional basis to incorporate the value of S_z. This is important to describe the entanglement of the triplet-pair state, for instance, and would, in the future, be crucial for describing the dynamical loss of this entanglement through vibronic couplings. With this machinery in place, we test our model Hamiltonian parametrized at the CASSCF level of theory with the adiabats obtained directly from dimeric ab initio calculations. Following verification of the qualitative features, we demonstrated the efficiency of the method in trying to understand the structure of larger aggregates. We predict and explore the spectra of aggregates along the $\vec{a}$ and herringbone directions.

The particular diabatic basis used to describe an aggregate is highly dependent on the system and phenomena at hand. While for this specific problem, we have chosen the basis accordingly, one could choose a different optimal set of basis sets and Hamiltonian to understand a different phenomenon. Our CASSCF calculations on the dimeric system at various distances reveal significant contributions from monomeric states with multiexcitonic character or di-ionic character. Including the spin-resolved versions of these states would bring higher accuracy to the tensor network results for the aggregates, but at a much greater computational cost. Future work would focus on incorporating more elaborate monomeric Hilbert spaces and vibronic interactions through Holstein-like interaction terms. Furthermore, the ultimate goal would be to use these effective Hamiltonians and knowledge from the resulting spectrum into a complete dynamical description of the phenomena. Comparative study of the singlet fission dynamics of such carefully modeled Hamiltonians at fully quantum mechanical and various semiclassical and quantum-classical levels of theory would be key to developing mechanistic insights into the processes. Work in this direction is also underway.

■ ASSOCIATED CONTENT

Supporting Information

The Supporting Information is available free of charge at https://pubs.acs.org/doi/10.1021/acs.jctc.6c00429.

> Comprehensive computational details and extended results supporting the main text, including adiabatic dimer excited states, Hamiltonian parametrization methodology, excitonic spectra along the $\vec{a}$ direction, CASSCF/RASSCF computational protocols, and characterization and convergence analysis of excited states in the 100-mer aggregate with periodic boundary conditions (PDF)

■ AUTHOR INFORMATION

Corresponding Authors

Amartya Bose − *Department of Chemical Science, Tata Institute of Fundamental Research, Mumbai 400005, India;* orcid.org/0000-0003-0685-5096; Email: amartya.bose@tifr.res.in

Debashree Ghosh − *School of Chemical Sciences, Indian Association for the Cultivation of Science, Kolkata 700032, India;* orcid.org/0000-0003-0726-7878; Email: pcdg@iacs.res.in

Author

Supriyo Santra − *School of Chemical Sciences, Indian Association for the Cultivation of Science, Kolkata 700032, India;* orcid.org/0000-0003-4884-2250

Complete contact information is available at: https://pubs.acs.org/10.1021/acs.jctc.6c00429

Notes

The authors declare no competing financial interest.

■ ACKNOWLEDGMENTS

S.S. thanks DST-Inspire for fellowship and IACS for computational facilities. D.G. thanks the ANRF-CRG grant (CRG/2023/001806) for funding. A.B. thanks TIFR for providing access to computational facilities.

■ REFERENCES

(1) Smith, M. B.; Michl, J. Singlet fission. *Chem. Rev.* **2010**, *110*, 6891−6936.

(2) Smith, M. B.; Michl, J. Recent advances in singlet fission. *Annu. Rev. Phys. Chem.* **2013**, *64*, 361−386.

(3) Breen, I.; Tempelaar, R.; Bizimana, L. A.; Kloss, B.; Reichman, D. R.; Turner, D. B. Triplet separation drives singlet fission after femtosecond correlated triplet pair production in rubrene. *J. Am. Chem. Soc.* **2017**, *139*, 11745−11751.

(4) Rao, A.; Friend, R. H. Harnessing singlet exciton fission to break the Shockley−Queisser limit. *Nat. Rev. Mater.* **2017**, *2*, 17063.

(5) Wilson, M. W.; Rao, A.; Ehrler, B.; Friend, R. H. Singlet exciton fission in polycrystalline pentacene: from photophysics toward devices. *Accounts of chemical research* **2013**, *46*, 1330−1338.

(6) Zeng, T.; Hoffmann, R.; Ananth, N. The low-lying electronic states of pentacene and their roles in singlet fission. *J. Am. Chem. Soc.* **2014**, *136*, 5755−5764.

(7) Monahan, N.; Zhu, X.-Y. Charge transfer−mediated singlet fission. *Annu. Rev. Phys. Chem.* **2015**, *66*, 601−618.

(8) Berkelbach, T. C.; Hybertsen, M. S.; Reichman, D. R. Microscopic theory of singlet exciton fission. II. Application to pentacene dimers and the role of superexchange. *J. Chem. Phys.* **2013**, *138*, 114103.

(9) Casanova, D. Theoretical modeling of singlet fission. *Chem. Rev.* **2018**, *118*, 7164−7207.

(10) Yost, S. R.; Lee, J.; Wilson, M. W.; Wu, T.; McMahon, D. P.; Parkhurst, R. R.; Thompson, N. J.; Congreve, D. N.; Rao, A.; Johnson, K.; et al. A transferable model for singlet-fission kinetics. *Nature Chem.* **2014**, *6*, 492−497.

(11) Santra, S.; Ray, J.; Ghosh, D. Mechanism of singlet fission in carotenoids from a polyene model system. *J. Phys. Chem. Lett.* **2022**, *13*, 6800−6805.

(12) Santra, S.; Ghosh, D. Unraveling the Geometrical Effects on Singlet Fission of Carotenoids: A Model Perspective. *J. Phys. Chem. A* **2025**, *129*, 2738−2744.

(13) Peng, B.; Wang, Z.; Jiang, J.; Huang, Y.; Liu, W. Investigation of ultrafast intermediate states during singlet fission in lycopene H-aggregate using femtosecond stimulated Raman spectroscopy. *J. Chem. Phys.* **2024**, *160*, 194304.

(14) Barford, W. Singlet Fission in Lycopene H-Aggregates. *J. Phys. Chem. Lett.* **2023**, *14*, 9842−9847.

(15) Barford, W.; Chambers, C. A. Theory of singlet fission in carotenoid dimers. *J. Chem. Phys.* **2023**, *159*, No. 084116.

(16) Coto, P. B.; Sharifzadeh, S.; Neaton, J. B.; Thoss, M. Low-lying electronic excited states of pentacene oligomers: A comparative electronic structure study in the context of singlet fission. *J. Chem. Theory Comput.* **2015**, *11*, 147−156.

(17) Japahuge, A.; Zeng, T. Theoretical studies of singlet fission: Searching for materials and exploring mechanisms. *ChemPlusChem.* **2018**, *83*, 146−182.

(18) Aryanpour, K.; Shukla, A.; Mazumdar, S. Theory of singlet fission in polyenes, acene crystals, and covalently linked acene dimers. *J. Phys. Chem. C* **2015**, *119*, 6966−6979.
(19) López-Carballeira, D.; Casanova, D.; Ruipérez, F. Theoretical design of conjugated diradicaloids as singlet fission sensitizers: quinones and methylene derivatives. *Phys. Chem. Chem. Phys.* **2017**, *19*, 30227−30238.
(20) Lim, S.-H.; Bjorklund, T. G.; Spano, F. C.; Bardeen, C. J. Exciton delocalization and superradiance in tetracene thin films and nanoaggregates. *Physical review letters* **2004**, *92*, No. 107402.
(21) Casanova, D. Bright fission: Singlet fission into a pair of emitting states. *J. Chem. Theory Comput.* **2015**, *11*, 2642−2650.
(22) Casanova, D. Electronic structure study of singlet fission in tetracene derivatives. *J. Chem. Theory Comput.* **2014**, *10*, 324−334.
(23) Zimmerman, P. M.; Bell, F.; Casanova, D.; Head-Gordon, M. Mechanism for singlet fission in pentacene and tetracene: From single exciton to two triplets. *J. Am. Chem. Soc.* **2011**, *133*, 19944−19952.
(24) Suarez, L. E. A.; de Graaf, C.; Faraji, S. Influence of the crystal packing in singlet fission: one step beyond the gas phase approximation. *Phys. Chem. Chem. Phys.* **2021**, *23*, 14164−14177.
(25) Plötz, P.-A.; Niehaus, T.; Kühn, O. A new efficient method for calculation of Frenkel exciton parameters in molecular aggregates. *J. Chem. Phys.* **2014**, *140*, 174101.
(26) Canola, S.; Bagnara, G.; Dai, Y.; Ricci, G.; Calzolari, A.; Negri, F. Addressing the Frenkel and charge transfer character of exciton states with a model Hamiltonian based on dimer calculations: Application to large aggregates of perylene bisimide. *J. Chem. Phys.* **2021**, *154*, 124101.
(27) Krieger, J.; Plasser, F. Rationalising Exciton Interactions in Aggregates Based on the Transition Density. *Chem. − Eur. J.* **2025**, *31*, No. e01570.
(28) Pitesa, T.; Polonius, S.; González, L.; Mai, S. Excitonic configuration interaction: Going beyond the Frenkel exciton model. *J. Chem. Theory Comput.* **2024**, *20*, 5609−5634.
(29) Pitesa, T.; Mai, S.; González, L. Efficient Excitonic Configuration Interaction for Large-Scale Multichromophoric Systems Using the Resolution-of-Identity Approximation. *J. Phys. Chem. Lett.* **2025**, *16*, 2800−2807.
(30) Nottoli, M.; Cupellini, L.; Lipparini, F.; Granucci, G.; Mennucci, B. Multiscale models for light-driven processes. *Annu. Rev. Phys. Chem.* **2021**, *72*, 489−513.
(31) Nelson, T. R.; White, A. J.; Bjorgaard, J. A.; Sifain, A. E.; Zhang, Y.; Nebgen, B.; Fernandez-Alberti, S.; Mozyrsky, D.; Roitberg, A. E.; Tretiak, S. Non-adiabatic excited-state molecular dynamics: Theory and applications for modeling photophysics in extended molecular materials. *Chem. Rev.* **2020**, *120*, 2215−2287.
(32) Gil, E. S.; Granucci, G.; Persico, M. Surface hopping dynamics with the Frenkel exciton model in a semiempirical framework. *J. Chem. Theory Comput.* **2021**, *17*, 7373−7383.
(33) Sangiogo Gil, E.; Giustini, A.; Accomasso, D.; Granucci, G. Excitonic approach for nonadiabatic dynamics: Extending beyond the Frenkel exciton model. *J. Chem. Theory Comput.* **2024**, *20*, 8437−8449.
(34) Hernández, F. J.; Crespo-Otero, R. Modeling excited states of molecular organic aggregates for optoelectronics. *Annu. Rev. Phys. Chem.* **2023**, *74*, 547−571.
(35) Zang, H.; Ke, Y.; Zhao, Y.; Liang, W. Effects of charge transfer state and exciton migration on singlet fission dynamics in organic aggregates. *J. Phys. Chem. C* **2016**, *120*, 13351−13359.
(36) Li, X.; Parrish, R. M.; Martínez, T. J. An ab initio exciton model for singlet fission. *J. Chem. Phys.* **2020**, *153*. 184116
(37) Mayhall, N. J. From model Hamiltonians to ab initio Hamiltonians and back again: Using single excitation quantum chemistry methods to find multiexciton states in singlet fission materials. *J. Chem. Theory Comput.* **2016**, *12*, 4263−4273.
(38) Li, X.; Parrish, R. M.; Liu, F.; Kokkila Schumacher, S. I.; Martínez, T. J. An ab initio exciton model including charge-transfer excited states. *J. Chem. Theory Comput.* **2017**, *13*, 3493−3504.
(39) Parker, S. M.; Seideman, T.; Ratner, M. A.; Shiozaki, T. Model Hamiltonian analysis of singlet fission from first principles. *J. Phys. Chem. C* **2014**, *118*, 12700−12705.
(40) Stan, I.-O.; Straatsma, T.; Broer, R.; de Graaf, C.; López, X. NOCI-F Electronic Couplings in Assemblies of Indolonaphthyridine Molecules: From Dimers to the Full Stack. *J. Chem. Theory Comput.* **2026**, *22*, 1296−1311.
(41) Havlas, Z.; Michl, J. Guidance for mutual disposition of chromophores for singlet fission. *Isr. J. Chem.* **2016**, *56*, 96−106.
(42) Zaykov, A.; Felkel, P.; Buchanan, E. A.; Jovanovic, M.; Havenith, R. W.; Kathir, R.; Broer, R.; Havlas, Z.; Michl, J. Singlet fission rate: Optimized packing of a molecular pair. Ethylene as a model. *J. Am. Chem. Soc.* **2019**, *141*, 17729−17743.
(43) Nishio, S.; Kurashige, Y. Rank-one basis made from matrix-product states for a low-rank approximation of molecular aggregates. *J. Chem. Phys.* **2019**, *151*, No. 084110.
(44) Schiefer, S.; Huth, M.; Dobrinevski, A.; Nickel, B. Determination of the crystal structure of substrate-induced pentacene polymorphs in fiber structured thin films. *J. Am. Chem. Soc.* **2007**, *129*, 10316−10317.
(45) Pipek, J.; Mezey, P. G. A fast intrinsic localization procedure applicable for ab initio and semiempirical linear combination of atomic orbital wave functions. *J. Chem. Phys.* **1989**, *90*, 4916−4926.
(46) Werner, H.; Knowles, P.; Knizia, G.; Manby, F.; Schütz, M.; Celani, P.; Györffy, W.; Kats, D.; Korona, T.; Lindh, R.et al.Molpro, version 2015.1, a package of *ab initio* programs, 2015.
(47) Deng, G.-H.; Brown, J. B.; Fisher, H.; Huang-Fu, Z.-C.; Qian, Y.; Zhang, T.; Harutyunyan, A.; Chen, H.; Chen, G.; Rao, Y. The anisotropic nature of singlet fission in single crystalline organic semiconductors. *Chem. Phys. Rev.* **2023**, *4*, No. 041313.
(48) Lubert-Perquel, D.; Szumska, A. A.; Azzouzi, M.; Salvadori, E.; Ruloff, S.; Kay, C. M.; Nelson, J.; Heutz, S. Structure dependence of kinetic and thermodynamic parameters in singlet fission processes. *J. Phys. Chem. Lett.* **2020**, *11*, 9557−9565.
(49) Berkelbach, T. C.; Hybertsen, M. S.; Reichman, D. R. Microscopic theory of singlet exciton fission. I. General formulation. *J. Chem. Phys.* **2013**, *138*, 114102.

https://doi.org/10.1021/acs.jctc.6c00429
J. Chem. Theory Comput. XXXX, XXX, XXX−XXX